Broadband sum-frequency generation as an efficient two-photon detector for optical tomography

Avi Pe'er*, Yaron Bromberg, Barak Dayan, Yaron Silberberg and Asher A. Friesem

Dept. of Physics of Complex Systems, Weizmann Institute of Science, Rehovot 76100, Israel
**Corresponding author: avi.peer@jila.colorado.edu*

Abstract: We describe a novel non-linear detection method for optical tomography that does not rely on detection of interference fringes and is free of optical background. The method exploits temporally coherent broadband illumination such as ultrashort pulses, and a non-linear two-photon detection process such as sum-frequency generation (SFG). At the detection stage, the reference beam and the sample beam are mixed in a *thick* non-linear crystal, and only the mixing term, which is free of optical background, is detected. Consequently, the noise limitations posed by the background in standard OCT (excess and shot noise), do not exist here. Due to the non-linearity, the signal to noise ratio scales more favorably with the optical power compared to standard OCT, yielding an inherent improvement for high speed tomographic scans. Careful design of phase matching in the crystal enables non-linear mixing which is both highly efficient and broadband, yielding both high sensitivity and high depth resolution.

OCIS codes: (190.7220) Upconversion; (110.4500) Optical coherence tomography;

References and links

1. D. W. Piston, "Imaging living cells and tissues by two-photon excitation microscopy," Trends Cell Biol. **9**, 66-69 (1999).
2. Y. Barad, H. Eisenberg, M. Horowitz, and Y. Silberberg, "Nonlinear scanning laser microscopy by third harmonic generation," Appl. Phys. Lett. **70**, 922-924 (1997).
3. D. Yelin, D. Oron, E. Korkotian, M. Segal and Y. Silberberg, "Third-harmonic microscopy with a titanium-sapphire laser," Appl. Phys. B **74**, 97-101 (2002).
4. J. Cheng, A. Volkmer, L.D. Book and X.S Xie, "An epi-detected coherent anti-Stokes Raman scattering (E-CARS) microscope with high spectral resolution and high sensitivity". J. Phys. Chem. B **105**, 1277-1280 (2001).
5. N. Dudovich, D. Oron and Y. Silberberg, "Single-pulse coherently controlled nonlinear Raman spectroscopy and microscopy," Nature **418**, 512-514 (2002).
6. D. Huang, E. A. Swanson, C. P. Lin, J. S. Schuman, W. G. Stinson, W. Chang, M. R. Hee, T. Flotte, K. Gregory, C. A. Puliafito, and J. G. Fujimoto, "Optical coherence tomography," Science **254**, 1178-1181 (1991).
7. A. F. Fercher, W. Drexler, C. K. Hitzenberger and T. Lasser, "Optical coherence tomography - principles and applications," Rep. Prog. Phys. **66**, 239-303 (2003).
8. Andrew M. Rollins, Joseph A. Izatt, "Optimal interferometer designs for optical coherence tomography," Opt. Lett. **24**, 1484-1486 (1999).
9. R. V. Sorin, D. M. Baney, "A simple intensity noise reduction technique for optical low coherence reflectometry," IEEE Photon. Technol. Lett. 4, 1404-1406, (1992).
10. J. G. Fujimoto, S. De Silvestri, E. P. Ippen, C. A. Puliafito, R. Margolis and A. Oseroff, "Femtosecond optical ranging in biological systems," Opt. Lett. **11**, 150-152 (1986).
11. C. Yan and J. Diels, "Imaging with femtosecond pulses," Appl. Opt. **31**, 6869-6873 (1992).
12. B. Dayan, A. Pe'er, A. A. Friesem and Y. Silberberg, "Coherent control with broadband squeezed vacuum," quant-ph/0302038.
13. B. Dayan, A. Pe'er, A. A. Friesem and Y. Silberberg, "Two photon absorption and coherent control with broadband down-converted light," Phys. Rev. Lett. **93**, 023005 (2004).

#81723 - $15.00 USD Received 2 Apr 2007; revised 24 May 2007; accepted 29 May 2007; published 28 Jun 2007

14. A. F. Fercher, C. K. Hitzenberger, G. Kamp, and S. Y. El-Zaiat, "Measurement of intraocular distances by backscattering spectral interferometry," Opt. Commun. **117**, 43–48 (1995).
15. M. A. Choma, M. V. Sarunic, C. Y., and J. A. Izatt, " Sensitivity advantage of swept source and Fourier domain optical coherence tomography," Opt. Express. **11**, 2183 (2003).
16. A. Yariv, *Quantum Electronics* (John Wiley and Sons, 1988, 3rd ed.), Chap. 16.
17. H. Wang, A. M. Weiner, "Efficiency of short-pulse type-I second-harmonic generation with simultaneous spatial walk-off, temporal walk-off, and pump depletion," IEEE J. Quantum Electron. 3**9**, 1600-1618 (2003).
18. A. P. Vandevender and P. G. Kwiat, "High efficiency single photon detection via frequency up-conversion," J. Mod. Opt **51**, 1433-1445 (2004).
19. D. Meshulach and Y. Silberberg, "Coherent quantum control of two-photon transitions by a femtosecond laser pulse," Nature **396**, 239-242 (1998).
20. Z. Zheng and A. M. Weiner, "Spectral phase correlation of coded femtosecond pulses by second-harmonic generation in thick nonlinear crystals," Opt. Lett. **25,** 984-986 (2000).
21. A. Pe'er, Y. Silberberg, B. Dayan, and A. A. Friesem, "Design of a high-power continuous source of broadband down-converted light," Phys. Rev. A. **74**, 053805 (2006).
22. K. König, T. W. Becker, P. Fischer, I. Riemann, and K.-J. Halbhuber, "Pulse-length dependence of cellular response to intense near-infrared laser pulses in multiphoton microscopes," Opt. Lett. **24**, 113-115 (1999).
23. A. F. Abouraddy, M. B. Nasr, B. E. A. Saleh, A. V. Sergienko and M. C. Teich, "Quantum-optical coherence tomography with dispersion cancellation," Phys. Rev. A 65, 053817 (2002).
24. M. B. Nasr, B. E. A. Saleh, A. V. Sergienko and M. C. Teich, "Demonstration of Dispersion-Canceled Quantum-Optical Coherence Tomography," Phys. Rev. Lett. **91**, 083601 (2003).
25. C. K. Hong and Z. Y. Ou and and L. Mandel, "Measurement of subpicosecond time intervals between two photons by interference," Phys. Rev. Lett. **59**, 2044-2047 (1987).

1. Introduction

The need for imagery with very high depth resolution of scattering media, such as biological samples, has led to the development of non-linear optical microscopy and optical coherence tomography [1-7]. Exploiting non-linear effects, has led to improved depth and lateral resolutions in microscopic imagery, where several prominent examples are two-photon microscopy [1], third harmonic microscopy [2,3] and CARS (coherent anti-Stokes Raman scattering) microscopy [4,5]. Unfortunately, non-linear microscopy typically requires high intensities, which in turn may damage the biological sample. Optical coherence tomography (OCT), on the other hand, utilizes only linear elastic scattering in the sample, so high intensities are not necessary [6-7]. In OCT the light reflected from the sample interferes with a delayed reference beam, whereby interference fringes appear only when the relative delay is within the coherence length of the light source. In order to achieve high depth resolutions, a light source with a short coherence length (large bandwidth) is best [7].

OCT uses heterodyne detection, which is advantageous for overcoming the detector noise. Yet, heterodyne detection has two inherent limitations. First, the detected interference pattern rides over an optical background that suffers from quantum shot noise and from excess noise [8,9]. While excess noise can be reduced (with some cost in dynamic range) by optimization of the reference beam intensity and by balanced detection [8], quantum shot noise of the reference beam sets an inherent limit on the signal to noise ratio (SNR) in OCT. Second, since OCT detects interference fringes, it is interferometrically sensitive to movements of the sample during the detection time. Thus, even though the depth resolution may be larger than the optical wavelength (5-10 microns typically), sub-wavelength movements of the sample cannot be tolerated. As a result, integration times in OCT must remain short compared to the typical uncontrolled movement time of the (sometimes living) imaged sample.

2. Basic concept

To overcome the above limitations of OCT, we consider a non-linear detection scheme that exploits broadband temporally coherent illumination. A prominent example for such a source is a mode locked laser emitting short pulses, and in order to simplify the presentation of the

#81723 - $15.00 USD Received 2 Apr 2007; revised 24 May 2007; accepted 29 May 2007; published 28 Jun 2007

concept we will consider this case first. However, ultrashort pulses are only one specific case out of a number of possible illumination sources, as we will later explain.

The basic configuration of our scheme is shown in Fig. 1. Here, a source of ultrashort pulses is used to generate two correlated pulse beams: a sample beam, which is elastically scattered from the sample, and a reference beam just like in conventional OCT. However, as opposed to conventional OCT, where the two beams are directly interfered on a photo-detector, here the two beams are first mixed in a nonlinear medium, where sum-frequency generation (SFG) is induced, and only the result of this mixing is detected in a process very similar to cross correlation of ultrashort pulses (the differences will be clarified later). When a short pulse impinges on the sample, the back scattered beam contains a train of pulses, whose temporal profile reflects the scattering profile of the sample along the beam path. The (weak) scattered pulse-train is mixed with the strong reference pulse in the non linear medium, and the resulting SFG photons are detected to obtain the temporal profile. It is clear that SFG will be generated only if the reference pulse overlaps temporally with a sample pulse. When the pulses do not overlap, no mixing can occur, so the detected SFG signal as a function of the reference delay reflects exactly the required scattering profile, with no optical background.

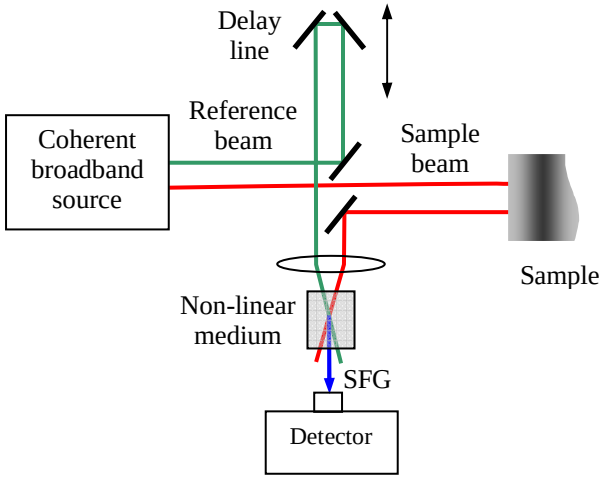

Fig. 1. Basic non linear OCT configuration. The sample and the reference beams are broadband with a coherent phase relation between them. The two beams are mixed non-linearly and the mixing term is detected as a function of the relative delay between the two beams.

The idea of using pulse cross-correlation for tomography is well known and even precedes that of time-domain OCT [10,11]. The problem with standard pulse correlation is that it requires broad phase matching for both the input pulses and the output SFG. As a result, the non-linear medium must be very thin, so the SFG efficiency is inherently low. We propose, however, to obtain highly efficient SFG in a thick non-linear crystal, without compromising the depth resolution. Indeed, for good depth resolution it is necessary that the non-linear interaction will coherently exploit the entire broad bandwidth of both beams. However, since here we are not interested in detecting the optical phase of the input fields, the resulting SFG signal need not be broad; in fact, it can be arbitrarily narrow. Only the input bandwidth that coherently contributes to this SFG signal should be broad; i.e. many frequency pairs need to be phase matched to sum up to the same SFG wavelength. This process is just the reversed equivalent of broadband parametric down conversion from a narrow pump. It can indeed be performed in thick, efficient nonlinear media and can achieve very high depth resolutions with type-I phase matching (in which the sample and reference beams have the same polarization) [12,13].

#81723 - $15.00 USD Received 2 Apr 2007; revised 24 May 2007; accepted 29 May 2007; published 28 Jun 2007

3. Performance analysis

The performance of an OCT setup is usually characterized by the signal-to-noise ratio (SNR), the sensitivity S, defined as one over the minimum detectable sample-reflectivity $R_{s,min}$, and by the dynamic range of detection. In standard OCT, the noise properties of the optical background (mostly due to the reference beam), pose the inherent limit on performance. In our coherent two-photon OCT (TP-OCT) method, only the cross term between the sample and the reference beams is measured, so the optical background (and hence optical noise) is absent, thereby performance can be improved. Specifically, while in standard OCT, the intensity noise of the reference beam is translated directly into phase noise in the interferometric measurement, in our method the reference serves only as a mechanism for conversion of sample photons into SFG photons, so its noise properties are almost irrelevant. Table 1 compares the expected performance of our TP-OCT with the ideal case of shot noise limited time-domain OCT (TD-OCT), under the common assumption of a very weak reflection from the sample, so its noise contribution is ignored (we will revisit this assumption later on).

Table 1. Expected performance of TD-OCT and TP-OCT

	TD-OCT [a]	TP-OCT
Signal	$\frac{\gamma_{TD}}{\hbar\omega}\sqrt{2P_R R_R P_S R_S}$	$\eta_{SFG}\gamma_{TP}\frac{P_S R_S}{\hbar\omega}$
Noise	$\sqrt{\frac{2\gamma_{TD}}{\hbar\omega}P_R R_R B}$	$\frac{NEP\sqrt{B}}{2\hbar\omega}$
SNR	$\sqrt{\frac{\gamma_{TD}}{\hbar\omega}\frac{P_S R_S}{B}}$	$\frac{2\eta_{SFG}\gamma_{TP}P_S R_S}{NEP\sqrt{B}}$
Sensitivity (*See text)	$\frac{\gamma_{TD}}{\hbar\omega}\frac{P_S}{B}$	$\frac{2\eta_{SFG}\gamma_{TP}P_S}{NEP\sqrt{B}}$

[a] From [8,9]

Comparison between TD-OCT and TP-OCT in terms of the signal, noise, signal to noise ratio (SNR) and sensitivity (S). For the TD-OCT we assume an ideal shot-noise limited configuration. η_{SFG} is the SFG quantum efficiency, γ_{TD} (γ_{TP}) is the quantum efficiency of the TD-OCT (TP-OCT) detectors, $\hbar\omega$ is the energy of the scattered photons from the sample, B is the electronic detection bandwidth, *NEP* is the noise equivalent power of the TP-OCT detector, Ps (P_R) is the power impinging on the sample (reference mirror) and Rs (R_R) is the sample (reference mirror) reflectivity.

Let us first compare the SNR of the two schemes. Due to the non-linear detection, the SNR scales more favorably with the sample power for TP-OCT. To demonstrate this, consider a simple, yet realistic case where the electronic noise floor in TP-OCT is similar to the shot noise level in TD-OCT and that the detection efficiencies are of order unity for both schemes (the SFG quantum efficiency η_{SFG}, defined as the probability of a sample photon to be up-converted to an SFG photon, can approach unity by selecting the appropriate reference intensity. For thick non-linear media this is easily achieved by current mode-locked laser oscillators). Accordingly, if the number of detected sample photons required to achieve a given SNR in standard TD-OCT is *N*, in TP-OCT it is only $\sqrt{N}$, thus allowing considerably faster scans or relaxed power requirement. Note that while the comparison to time-domain OCT is natural here since our method is the "two-photon" equivalent of TD-OCT, this SNR scaling argument is equally valid also for Fourier-Domain OCT [14,15].

#81723 - $15.00 USD Received 2 Apr 2007; revised 24 May 2007; accepted 29 May 2007; published 28 Jun 2007

Another important advantage for TP-OCT is that the SFG intensity directly reflects the depth information, whereas in standard OCT, reliable depth recovery requires detection of the interference fringes. Accordingly, TP-OCT is immune to the relative optical phase noise the two beams due to uncontrolled, sub-wavelength vibrations of the sample, which are deleterious for standard OCT. Thus, TP-OCT may offer an advantage for applications where long detection times (narrow bandwidths) are required with live, moving samples.

While it is common to neglect the noise properties of the sample beam due to the weakness of the sample reflections, it is important to realize that for *any imaging scheme* the ultimate limit on the scanning speed and sensitivity is set by the quantum nature of the sample light; i.e. at least one detected sample photon per detection time ($1/B$). Accordingly, even with extremely quiet, state of the art photon counting detectors (*NEP*s of order 10^{-18}W/Hz$^{1/2}$ and large detection bandwidths; e.g. 100KHz) it is impossible to detect below the 'one photon level'. Any attempt for sub-photon detection will inevitably yield degraded, 'photon-starved' images.

4. Details of the non-linear mixing

Let us examine the properties of the non-linear mixing a bit further. In the absence of phase matching restrictions (thin medium), the non-linear dipole P_{NL} (and the SFG field) excited in a medium with second order ($\chi^{(2)}$) non-linearity is proportional to the input field squared:

$$P_{NL} \propto \left(A_s(t)+A_r(t)\right)^2 = A_s^2(t)+A_r^2(t)+2A_s(t)A_r(t), \tag{1}$$

where A_s,A_r are the sample and reference fields respectively. Since we are only interested in the mixing term, we need to filter out the other two terms (mainly the one associated with the strong reference beam), so they will not contribute to the measured SFG signal. This can be achieved by separating the two beams either spectrally or spatially. If the sample and the reference beams are spectrally separated, then the three terms in Eq. (2) are also separated and the required term can be filtered out. Similarly, if the two beams arrive at different angles (a non-collinear interaction), the three resulting terms propagate in different directions and the mixing term can be spatially filtered. Note however that in most practical cases, where the interaction is performed in a thick crystal, only one of the terms is phase matched, so partial filtering occurs automatically.

In order to understand the effect of phase matching, let us rewrite the mixing term in the frequency domain, where the non-linear response can be expressed as a convolution of the two input fields and the phase matching function F_{pm} acts as a complex spectral filter [16]:

$$P_{NL}(\Omega) \propto \int d\omega A_s(\omega)A_r(\Omega-\omega)F_{pm}(\Omega,\omega), \tag{2}$$

$$F_{pm}(\Omega,\omega) = \exp[i\Delta k(\Omega,\omega)l/2]\frac{\sin[\Delta k(\Omega,\omega)l/2]}{\Delta k(\Omega,\omega)/2}, \tag{3}$$

with l the thickness of the medium, Δk the momentum mismatch and Ω,ω the SFG and input frequencies, respectively. The SFG can be efficient within the spectral bandwidth where the phase mismatch is small ($|\Delta k \cdot l| < \pi$). In a thick crystal with type-I phase matching, the dependence of the phase mismatch on the two frequencies Ω,ω can be very different. While the phase mismatch depends very steeply on Ω, the input bandwidth that efficiently contributes to a given Ω can be very large. Fig. 2 depicts the phase matching function F_{pm} in two cases: Figs. 2 (a), 2 (b) and 2 (c) correspond to the conditions later realized in the experiment, where a 14mm long BBO (β-Barium Borate) crystal was used with input pulses around 800nm. Note that despite the narrow bandwidth in Ω, 0.2 nm in this example, the sensitivity to relative delay remains as dictated by the broad input bandwidth, so high depth resolution is still achieved (less than 5.5μm). While in this example it may seem that the phase matching bandwidth sets a limit on the maximal depth resolution with our scheme, it is important to realize that much broader phase matching bandwidths can be obtained using wavelengths that are closer to the zero dispersion of the crystal [13]. Figs. 2 (d), 2 (e) and 2 (f)

#81723 - $15.00 USD Received 2 Apr 2007; revised 24 May 2007; accepted 29 May 2007; published 28 Jun 2007

depict exactly this situation in an LBO crystal of the same length at T=40°C (similar ultrabroad phase matching regions can be calculated also for other non-linear materials). Clearly it is possible to achieve input bandwidths approaching an octave in frequency, which can easily support depth resolution in the 1μm range.

The overall conversion efficiency is given by the up-conversion bandwidth multiplied by the conversion efficiency per SFG spectral component. While the up-conversion bandwidth is inversely proportional to *l*, the conversion efficiency per spectral component has a nontrivial scaling with *l*, which in general depends on the focusing and on the spatial and temporal walk-offs between the fundamental and the second harmonic [17]. Careful analysis of the conversion efficiency as given in [17], shows that in terms of total SFG power, a thick medium is favorable. Fortunately, in long enough crystals (>1cm) and with a strong enough reference, the SFG efficiency can approach unity, as was previously demonstrated for detection of single photons in the infrared via SFG with a strong CW reference [18].

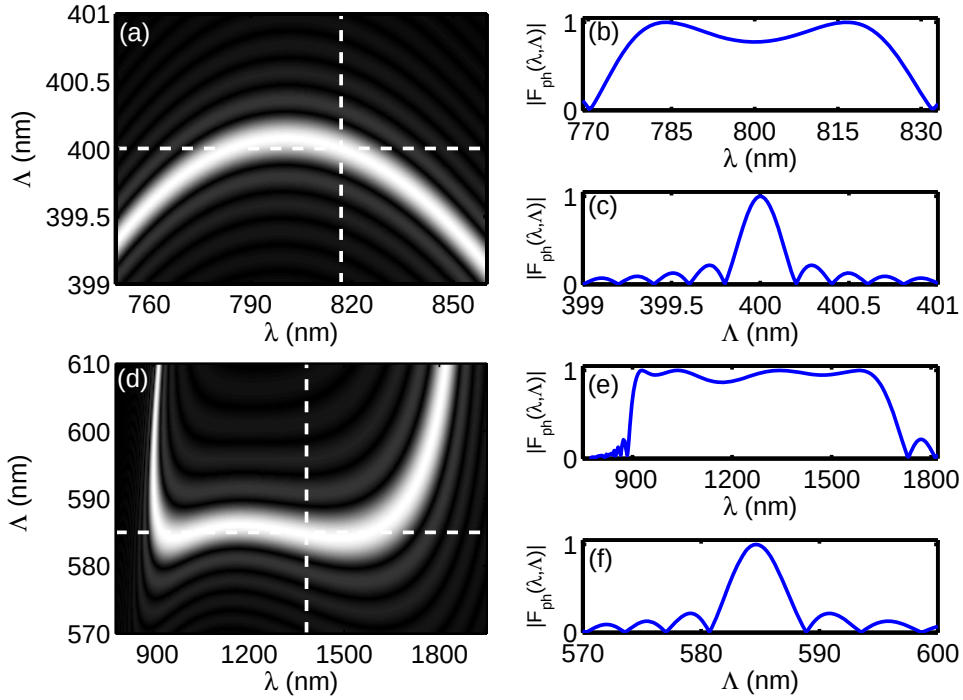

Fig. 2. Calculated phase matching function $|F_{pm}|$; (a) A 2-D density plot of $|F_{ph}|$ as a function of the input wavelength λ and the SFG wavelength Λ, for a 14mm long BBO crystal around 800nm with a non-collinear angle is of 1°. The cross sections along the marked dashed lines are shown in (b) (horizontal cross section) and (c) (vertical cross section). (d), (e) and (f) show similar plots for an LBO crystal with non-critical phase matching and T=40°C, demonstrating ultra-broad phase matching bandwidth near the zero dispersion of the non-linear medium.

Since the SFG output is narrowband in a thick crystal, it is not necessary for the input pulses to be transform limited. In order for the SFG at a given Ω to be efficient, all the input frequency pairs that sum up to it should interfere constructively (the integrand in Eq. (3) should have a constant phase). This is achieved by any pair of fields that fulfill [10,11,19,20]

$$A_s(\omega) = A_r^*(\Omega - \omega). \tag{4}$$

Consequently transform limited pulses are just one specific case out of many other possible correlated fields. An extreme example of the freedom of choice is that of broadband

#81723 - $15.00 USD Received 2 Apr 2007; revised 24 May 2007; accepted 29 May 2007; published 28 Jun 2007

parametric down conversion, where the two generated fields (the signal and the idler) are incoherent white noises, but their phases are coherently linked to exactly fulfill the above requirement [12,13,21]. In order to preserve the coherent phase relation between the beams it is necessary to compensate for dispersion in the sample beam by insertion of the opposite dispersion to the reference beam. In addition, it is possible to purposely avoid transform limited pulses that can cause multi-photon damage to the living sample by introducing strong opposite dispersions to the two beams.

5. Experimental proof-of-principle

To demonstrate the principles of our TP-OCT scheme, we utilized the experimental configuration, schematically shown in Fig. 3. Pulses of 45fs at 800nm (50 nm bandwidth) were emitted from a home built mode-locked Ti:Sapphire laser with 80 MHz repetition. The pulses were split on a polarizing beam splitter to a reference and a sample beam (each ~80 mW, average power). The reference beam was delayed, polarization rotated to match the sample beam, and spatially shifted with respect to the sample beam to enable non-collinear mixing in a 14mm long BBO crystal. The broad phase matching of the BBO (shown in Figs. 2 (a), 2 (b) and 2 (c)) enables an efficient conversion of the entire 50 nm bandwidth, which corresponds to a maximum depth resolution of 5.7 μm. In the horizontal axis both walk-off and non-colinearity limit the focusing (reduce beam overlap), so a weak cylindrical lens (f=50 cm) was used, whereas for the vertical axis the focusing is limited only by the angular acceptance dictated by phase matching, so the focal length was chosen to yield a Rayleigh range comparable with the length of the crystal (f=16 cm). The non collinear angle is chosen to be 1°, to enable reasonable spatial filtering of the cross-SFG beam after the crystal.

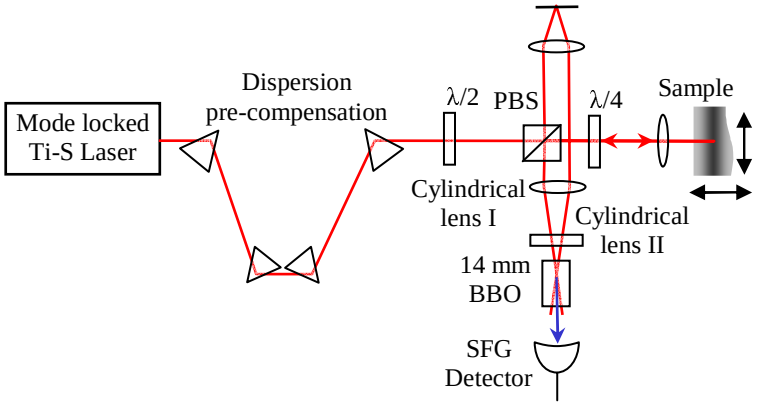

Fig. 3. Experimental configuration. Pulses of 45fs at 800nm, emitted from a home built mode locked Ti:Sapphire laser with 80 MHz repetition, were pre-compensated for dispersion with four prisms (SF57 glass) and then split using a polarizing beam splitter (PBS) to a sample beam and a reference beam (the ratio between the beams was set by the angle of the half wave plate). The delay of the reference beam was tuned manually and the sample was mounted on a 3-axis motorized stage. The sample beam is focused with a f=20 mm lens onto the sample, yielding a focal spot of ~5 μm. A double pass of the sample beam through a quarter wave plate rotated its polarization so it is reflected by the PBS towards the non-linear crystal (BBO, type-I phase matching). The first cylindrical lens weakly focuses the two beams to overlap at the BBO crystal (focal spot of ~250 μm) and the second cylindrical lens focuses tightly in the perpendicular direction for high efficiency (focal spot of ~30 μm). The cross SFG signal at 400 nm was then detected while the position of the sample was scanned in two dimensions. The SFG signal was collimated, filtered out from the infrared light by a polarizer and a prism (not shown here) and then detected with a Thorlabs silicon photodiode (3.6 mm wide active area). In order to avoid spurious zero level shifts from the detector, the sample beam was chopped and a lock-in amplifier was used for the detection.

With a mirror as a sample we measured the SFG efficiency η_{SFG}, which indicates the conversion efficiency of a sample photon into an SFG photon. At an average reference power

#81723 - $15.00 USD Received 2 Apr 2007; revised 24 May 2007; accepted 29 May 2007; published 28 Jun 2007

of 80 mW and sample power of 60 mW, the measured SFG efficiency was 8.5±0.3% (SFG measured power of 10.2±0.3 mW), as predicted by numerical calculation of the SFG field generated with short pulses [17]. For a collinear SFG configuration and optimal focusing conditions, we calculated efficiencies of 30% at these power levels. Obviously, with higher reference powers the conversion efficiency will also increase.

We now scanned the delay between the beams, in order to measure the depth resolution of our configuration. The obtained profile of the SFG signal, shown in Fig. 4, reflects the impulse response of the measurement to a single scatterer. As evident, a depth resolution of 6.5 μm is obtained, which is nearly transform limited based on the spectral bandwidth used. The low optical DC level at -60 dB is due to a residual SFG signal from the sample beam alone (the A_s^2 term in Eq. (2)), detected due to imperfect spatial filtering. However the optical noise level from this weak background is negligible compared to the electronic detection noise, and since this DC level scales as the sample beam intensity squared, for an actual sample with low reflectivity it will be totally negligible. The noise floor (-75 dB) of the measurement is indeed limited only by the electronic detection noise of the simple detector (Si photo-diode, NEP=10^{-11} W·(Hz)$^{-1/2}$) and the lock-in amplifier used (with a 20 ms integration time). The noise floor level agrees reasonably with the sensitivity of S=80 db calculated according to Table 1. By detecting the SFG signal with a single photon detector or a photon multiplier tube the sensitivity could improve by several orders of magnitude (e.g. for 10 mW power impinging on a sample, an SFG efficiency of 0.4, a *NEP* of $2\cdot10^{-18}$ W·(Hz)$^{-1/2}$ (typical for single photon detectors) and a detection bandwidth of 100 KHz we estimate a sensitivity of S=120 db).

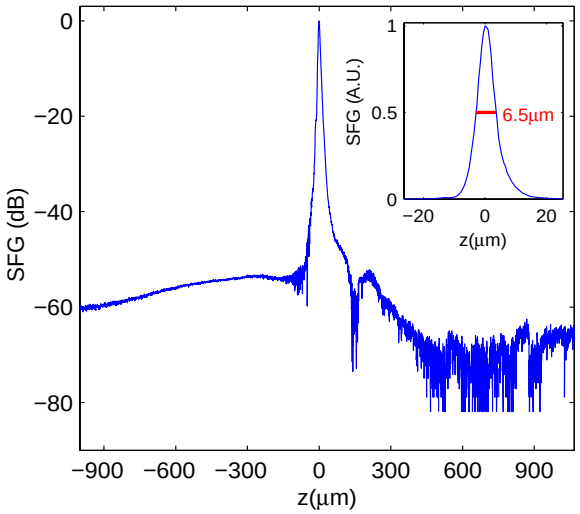

Fig. 4. Depth resolution measurement. The scattering profile of a single scatterer (mirror) measured along the optical (z) axis is shown on a log scale. The sharp profile is superimposed on a -60 dB residual SFG signal due to the sample beam, however the -75 dB noise level is dictated by the electronic detection noise only. The inset shows the scattering profile on a linear scale, demonstrating a resolution of 6.5 μm FWHM.

In order to qualitatively demonstrate the tomographic ability of the method, we imaged a two dimensional cut in the *XZ* plane (*Z* being the optical axis), of onion epithelium, as shown in Fig. 5 on a logarithmic intensity scale. The layered structure of the sample is clearly seen with high resolution to a depth deeper than 1mm. The average power delivered to the sample was 80 mW, which is well below the damage threshold for living cells with our pulse duration and focusing [22]. The maximal imaging depth was mostly limited by the high electronic detection noise of the photodiode detector and the lock-in amplifier used in our experiment.

#81723 - $15.00 USD Received 2 Apr 2007; revised 24 May 2007; accepted 29 May 2007; published 28 Jun 2007

Clearly with low noise, UV optimized detectors, deeper imaging at lower sample beam powers is possible. The measured SFG power in our experiment (about 0.15 mW for the peaks in Fig. 5) was high enough to support high speed, real-time scans, just as in commercial implementations of standard OCT. However, due to the use of slow translators for scanning the sample position, this was not demonstrated in our experiment (the total tomographic scan took several hours). While we cannot claim the image obtained in this preliminary demonstration to be superior to standard OCT images obtained under similar conditions, yet the tomographic ability is clearly demonstrated.

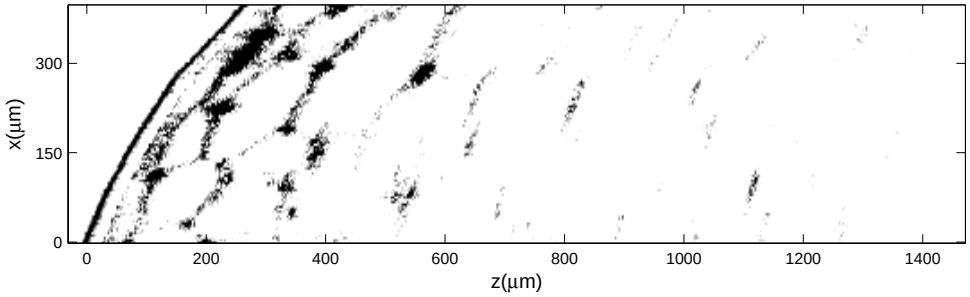

Fig. 5. A tomographic *XZ* cut of an onion epithelium, on a logaritmic scale. The internal layered structure is clearly seen to a depth of >1 mm.

6. Discussion and concluding remarks

Coherent two-photon OCT is related to quantum OCT [23,24], a method that relies on the quantum mechanical properties of time-energy entangled photon pairs emitted via broadband down-conversion. The method exploits the short correlation time of entangled photon pairs for depth resolution, and a Hong-Ou-Mandel (HOM) two-photon interferometer as the detecting device [25]. Since quantum OCT relies on the quantum properties of single photon pairs, it is inherently limited to operate at extremely low power levels so its practicality is questionable. While our method also relies on a coherent two-photon correlation, the use of broadband SFG as the two photon detector instead of HOM interference allows both a classical description of the phenomenon and the use of high, classical power levels, leading to a practical robust method.

An important feature of TP-OCT is that with a thick non-linear medium, where the SFG bandwidth is narrow, the sample and reference fields need not be transform limited pulses. They should only remain complex conjugates of each other. This design freedom allows one to diminish two-photon damage in the sample without reducing the SFG signal by purposely dispersing the sample beam, while introducing the opposite dispersion to the reference beam. Accordingly, one may consider the commercially attractive fiber based TP-OCT implementation, where normal fiber is used for the sample arm and standard dispersion compensating fiber in the reference arm. Alternatively, one can employ the same fiber for both beams, with the sample and reference beams wavelengths chosen symmetrically around the zero dispersion point of the fiber.

To conclude, we developed a new non-linear detection method for optical tomography, which relies on a temporally coherent broadband source and efficient broadband physical two-photon detection. The method offers high depth resolution along with immunity to uncontrolled vibrations for low speed scans and superior performance for high speed tomographic scans, limited only by electronic detection noise. We verified the efficiency of the method experimentally, showing that it is already possible to obtain depth resolution of about 6.5 microns and up-conversion efficiencies of 8.5%. We expect that the resolution and up-conversion efficiency can be improved by utilizing more elaborate phase matching configurations, by using non-linear media of even higher non-linearity, such as periodically polled crystals and by increasing the power of the reference beam. Superb SNR and dynamic

#81723 - $15.00 USD Received 2 Apr 2007; revised 24 May 2007; accepted 29 May 2007; published 28 Jun 2007

range can be reached by a combination of a high noise detector for the high intensities and a low noise detector for the single photons level.

#81723 - $15.00 USD Received 2 Apr 2007; revised 24 May 2007; accepted 29 May 2007; published 28 Jun 2007